Solution Structure of a Hexitol Nucleic Acid Duplex with Four Consecutive T·T Base Pairs

by **Eveline Lescrinier**[a]), **Robert M. Esnouf**[b]), **Jan Schraml**[c]), **Roger Busson**[a]), and **Piet Herdewijn***[a])[1])

[a]) Laboratory of Medicinal Chemistry, Rega Institute for Medical Research and Faculty of Pharmacy, Katholieke Universiteit Leuven, Minderbroedersstraat 10, B-3000 Leuven
[b]) Division of Structural Biology, Wellcome Trust Centre for Human Genetics, Roosevelt Drive, Headington, Oxford, OX3 7BN
[c]) Institute of Chemical Process Fundamentals, Rozvojova 135, 165 02 CZ-Prague 6

The structure of the hexitol nucleic acid (HNA) h(GCGCTTTTGCGC) was determined by NMR spectroscopy. This unnatural nucleic acid was developed as a mimic for *A*-RNA. In solution, the studied sequence is forming a symmetric double-stranded structure with four central consecutive T·T wobble pairs flanked by G·C *Watson-Crick* base pairs. The stem regions adopt an *A*-type helical structure. Discrete changes in backbone angles are altering the course of the helix axis in the internal loop region. Two H-bonds are formed in each wobble pair, and base stacking is preserved in the duplex, explaining the stability of the duplex. This structure elucidation provides information about the influence of a $(T)_4$ fragment on local helix geometries as well as on the nature of the T·T mismatch base pairing in a TTTT tract.

1. Introduction. – The sequence of RNA has an influence on its final three-dimensional structure. Due to frequently occurring base-pair mismatches, RNA is allowed to adopt secondary-structure motifs that are different from the typical *A*-form geometry of double-stranded RNA (dsRNA). Moreover, several RNA sequences have been shown to occur as equilibria between different structures. Among them, the hairpin-duplex equilibrium is most characteristic. Some of these conformations might be more biologically relevant than others, but when they represent only a minor part of the total RNA in solution, it is difficult to study their structure in detail. The fraction of noncanonical base pairs is estimated to 6% of all base pairs in ribosomal RNA, with 50% of those being G·G and 17% U·U [1]. The U·U base pair is very flexible, and it occurs frequently in RNA [2–4]. An analogous T·T mismatch is observed in DNA in the solution structure of $d(m^5CCTCC_2)$[5] and of other i-motifs [6] where T·T wobble pairs are formed between strands that are oriented parallel to each other. Therefore, mismatches can be considered as structural elements of nucleic acids rather than errors in sequences.

Both NMR-based solution structures and crystallographic structures of U·U-containing duplexes have been studied intensively. Self-complementary ribonucleic acids with U·U tandem mismatches often occur as duplexes. For example, the r(CGCUUGCG) sequence forms a stable duplex in 1M NaCl [7][8]. The X-ray structure of two noncanonical U·U base pairs flanked by C·G (CUUG) has been

[1]) Tel.: +32-16-33 73 87, Fax: +32-16-33 73 40, e-mail: Piet.Herdewijn@rega.kuleuven.ac.be

studied in r(GGCGCUUGCGUC). This dodecamer forms a hairpin loop at low salt concentration and a duplex structure under crystallization conditions [9]. The formation of an *A*-type duplex structure containing U · U wobble pairs in an internal loop causes only small changes in backbone angles and preserves base stacking in the helix. For both U · U base pairs, O(2) and N(3) of one uracil are H-bonded to N(3) and O(4) of the uracil base in the opposite strand. Interestingly, this base pairing alters the course of the helix axis by 11 – 12°.

The structure of a double-stranded helical RNA structure with an internal loop of two U · U mismatches flanked by U · G standard wobble pairs was determined by X-ray diffraction [10]. Superimposition of the crystallographic model onto a canonical *A*-form RNA structure showed that the central mismatches cause no major distortion of this helix. Both U · U mismatches form wobble pairs, but one of them is so highly twisted that only one H-bond can be formed. The loss of one H-bond is compensated by a potential intraresidue H-bond and by a bound H_2O molecule that bridges the two O(4) atoms of this wobble pair with two H-bonds.

Thermodynamic studies on loop formation in RNA tetraloops demonstrated biphasic melting points for the r(GGACUUUUGUCC) sequence, indicating the presence of significant amounts of two species – most likely hairpin and duplex structures. Other reported DNA [11] and RNA [12] sequences with four central T (DNA) or U (RNA) residues only adopt hairpin structures. So far, the structure of a UUUU tract in RNA has only been determined as a hairpin [13]. The formation of this hairpin structure implies conformational changes in backbone angles in the loop region.

The behavior of RNA is similar to that described for pyranosyl-RNA (pRNA) [14], a nucleoside analogue in which the five-membered ribose is replaced by a six-membered pyranose. The pRNA sequence pr(GCGTTCGC) forms a duplex. Increasing the number of thymine nucleotides at the center of the oligomer shifts the equilibrium toward the hairpin conformation. The pyranosyl sequence pr(GCGTTTTCGC) adopts an exclusive hairpin structure (at 0.15M NaCl) with a stability comparable to that of the corresponding RNA hairpin. These conclusions are derived from concentration-dependent melting temperature (T_m) measurements. Thus, neither flexible furanose nucleotides (*i.e.* ribose or deoxyribose) nor pyranosyl RNA can be used to study self-complementary duplexes with an internal loop formed by a UUUU or TTTT tract.

Folding a TTTT or UUUU sequence into a tetraloop hairpin requires an *S*-type sugar conformation to bridge the ends of an *A*-type stem with *N*-type sugars [15]. The formation of a hairpin structure might be avoided by using conformationally restricted nucleotides, where the carbohydrate moiety is not able to adopt an *S*-type conformation. Recently, we have synthesized hexitol nucleic acids (HNAs) as mimics of *A*-type RNA [16]. A HNA is a modified nucleic acid consisting of a phosphorylated 1,5-anhydrohexitol backbone and natural nucleobases (Fig. 1). HNAs are distinguished from pRNAs by having strong and selective hybridization properties with complementary natural nucleic acids. The building block of HNA (a 1,5-anhydrohexitol nucleotide) can be considered a conformationally restricted mimic of a natural nucleoside in its *N*-conformation [17]. The stiffness of the six-membered anhydrohexitol rings prevents HNAs from undergoing drastic conformational alterations. There-

fore, HNA can be used as a model nucleic acid in which folding into a TTTT (or UUUU) tetraloop is avoided.

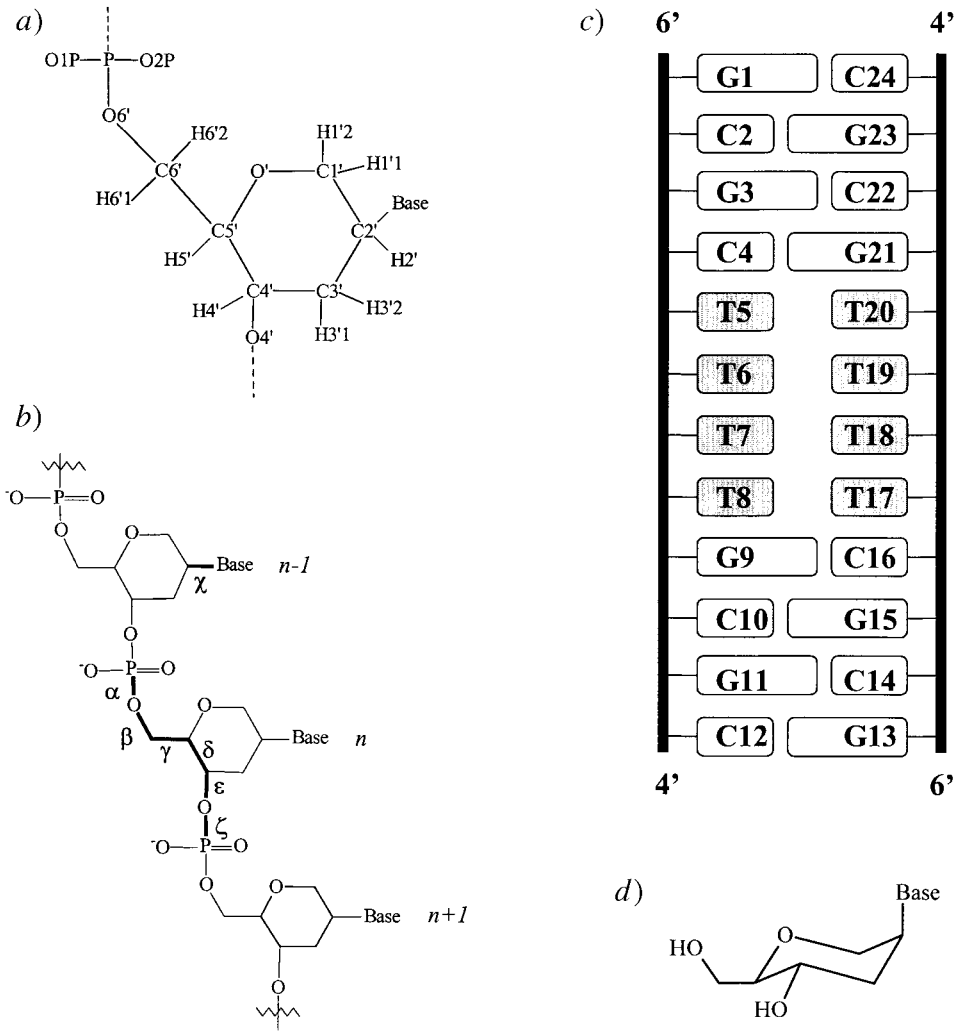

Fig. 1. a) *Chemical structure and atomic numbering in a HNA nucleotide* (base = guanine, cytosine, or thymine). b) *Schematic representation of a HNA oligonucleotide* (main torsion angles are indicated and labeled in boldface). c) *Diagram of dsHNA* (thymine bases forming the internal loop of non-standard base pairing are shaded). d) *Preferred conformation of HNA monomers as determined by X-ray crystallography and NMR spectroscopy.*

During studies of the hybridization properties of HNA, we observed that HNA oligothymidylate (oligo(hT)) self-associates at high NaCl concentrations (1M) in the presence of $MgCl_2$, but not at low NaCl concentrations (0.1M) [18–20]. Although neither the characterization of this hybridization nor the orientation of the oligo(hT)

strands were studied, this demonstrates the occurrence of T·T base pairing in HNA. Therefore, we studied the structure of the HNA oligomer h(GCGCTTTTGCGC) that adopts an *A*-type helix structure in solution with an internal loop formed by a TTTT tract. This structure elucidation could provide information about the influence of a $(T)_4$ fragment on local helix geometries as well as the nature of the T·T mismatch base pairing in a TTTT tract.

The NMR-derived structure we report here shows remarkable similarities to the crystal structure of r(GGCGUUGCGUC) [9]. This may indicate that the structure presented here could be considered a model for the duplex structure adopted by r(GGACUUUUGUCC), which cannot be determined due to its instability.

2. Results and Discussion. – 2.1. *Preamble.* The constitution of HNAs, their atom numbering, and the definitions of the main torsion angles are depicted in *Fig. 1, a* and *b*. Individual residues in the sequence studied (*Fig. 1, c*) are composed of six-membered 1,5-anhydrohexitol rings, substituted at C(2′) with nucleobases that can be either guanine (G), thymine (T), or cytosine (C). Adjacent residues are connected by a 4′(*n*) to 6′ (*n* + 1) phosphodiester linkage. Due to the C(2′) positioning of the base moiety, these nucleoside analogues lack an anomeric center. Replacement of the furanose ring by an anhydrohexitol ring results in a reduced conformational flexibility of the carbohydrate moiety of HNA compared to natural nucleic acids. The most stable conformation of HNA monomers, as determined by X-ray crystallography [21] and ^{1}H-NMR spectroscopy [22] is depicted in *Fig. 1, d*.

2.2. *Formation of the Duplex Structure.* A natural nucleic acid with sequence 5′-GCGCTTTTGCGC-3′ would be expected to adopt a hairpin structure. However, as explained above, HNA should not be able to fold similarly.

The one-dimensional (1D) ^{1}H-NMR spectrum of h(GCGCTTTTGCGC) in D_2O showed a mixture of two different conformations of the oligomer (*Fig. 2*, middle). Increasing temperature caused a decrease of one set of signals, while the second set simultaneously increased. At 70°, only one structural form could be observed (*Fig. 2*, top). This is probably the single-stranded HNA (ssHNA), since the T_m of h(GCGCTTTTGCGC) as a 4 μM solution in H_2O with 0.1M NaCl is 52°. When NaCl was gradually added to the sample at 20°, signals from ssHNA decreased, while those belonging to the second structural form increased. At 0.3M NaCl, only signals of the second structural form were visible in the 1D ^{1}H-NMR spectrum (*Fig. 2*, bottom). This sample was used for further studies, in which this structure was shown to be double-stranded HNA (dsHNA).

2.3. *Determination of the Duplex Structure.* The assignment of non-exchangeable protons was performed in two stages. First, ^{1}H-NMR signals of the HNA dodecamer were assigned by TOCSY, NOESY, and COSY. This assignment allowed the determination of the conformation for the twelve hexitol rings in the molecule. Second, the sequential assignment of residues based on interresidue NOE contacts was performed.

Expansions of a NOESY plot with mixing time 50 ms (*Fig. 3*) show the intraresidue NOE effects used to link the aromatic proton signals to a hexitol proton spin system (*Fig. 3, b*) and the observed interresidue $H^2-C(3')$ (= H3′2)(*n*) to H−C(8)/H−C(6)(= H8/H6)(*n* + 1) cross-peaks (*Fig. 3, a*) needed for sequential assignment in the dodecamer.

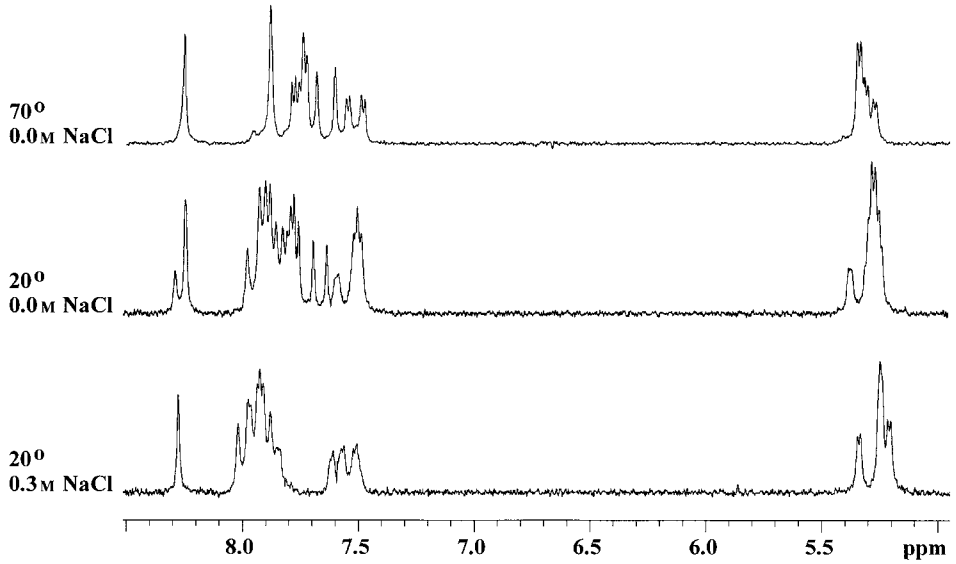

Fig. 2. *Section of the one-dimensional ^{1}H-NMR spectrum of a 2 mM solution of h(GCGCTTTTGCGC) in D_2O, measured under different experimental conditions*

The temperature dependence of imino-proton signals is depicted in *Fig. 4*. The four signals between 10 and 12 ppm are characteristic of two different T·T base pairs. This base-pairing evidence is corroborated by strong pairwise NOEs of these signals in a Watergate NOESY spectrum at 0°, used for sequential assignment of the imino signals (*Fig. 5*). The occurrence of T·T base pairing implied that, under the experimental conditions, h(GCGCTTTTGCGC) is forming a symmetrical duplex with four central T·T mismatches flanked by four G·C base pairs on each side. Due to the symmetry of the duplex, signals from both strands degenerate. Duplex formation is confirmed by the absence of a 'turning phosphate', which would be expected in a hairpin structure and which would show a downfield shift compared to phosphate signals in the duplex region of the hairpin stem. In this sample, all ^{31}P nuclei resonated within a 1 ppm range, suggesting that no large backbone distortion had occurred [23].

In one of the mismatch T·T pairs, a much larger spectral separation exists for the imino signals between 10 and 12 ppm compared to the separation for the second pair. In the Watergate NOESY spectrum, these separated signals were assigned to the hT5·hT20 and hT8·hT17 mismatches. This is in agreement with the description of tandem U·U mismatches in the sequence track 5′-YUUR-3′/5′-YUUR-3′ (R = G, Y = C or U) [7] that have one downfield shifted line at *ca.* 11.3 ppm and an upfield shifted imino signal at *ca.* 10.5 ppm. In a thorough NMR analysis of ^{15}N- and ^{13}C-labeled RNA in combination with multidimensional homo- and heteronuclear experiments [24], the downfield signal was assigned to the U-3′ neighbor of Y preceding the U·U wobble pairs. Difference in stacking and shielding effects in a more-or-less regular *A*-type RNA helix were considered possible reasons for the large spectral separation of both imino protons of the U·U mismatch. The similarity to this tandem U·U mismatch was used to assign the signal at 11.5 ppm to H−C(3) of hT5 and hT17 (the 4′ neighbors of hC4

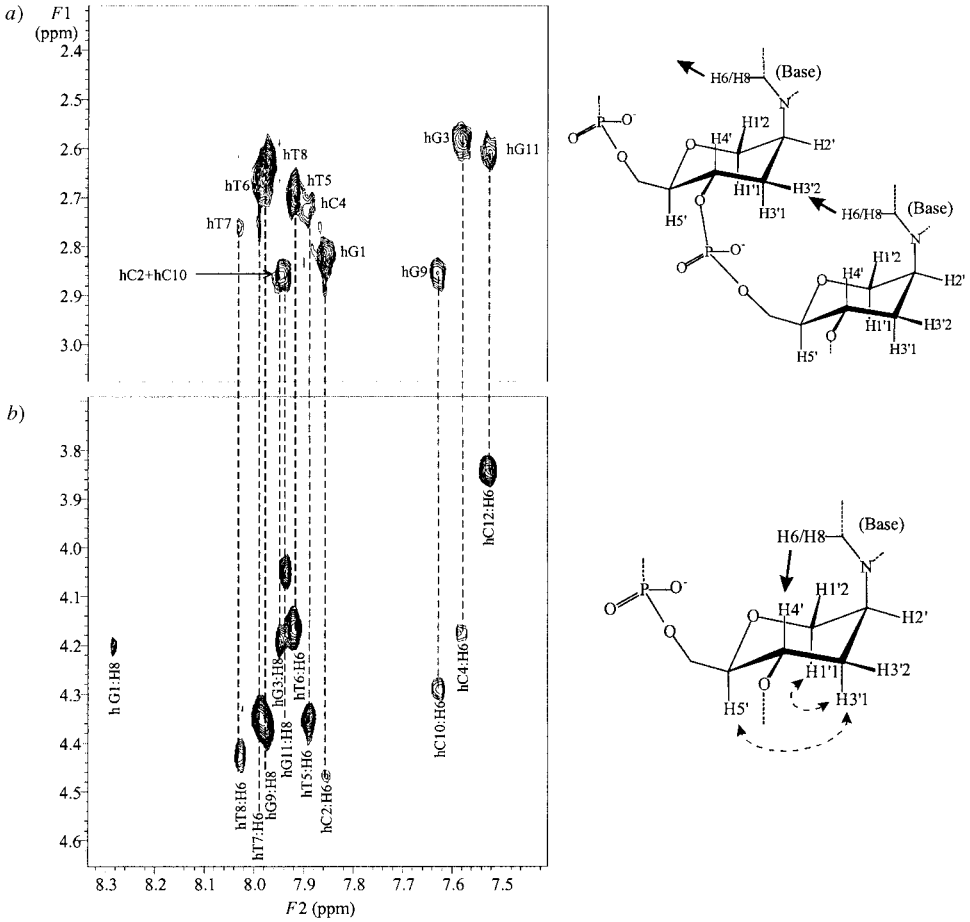

Fig. 3. *Expansions of a 50-ms mixing time NOESY spectrum of a 2 mM solution of h(GCGCTTTTGCGC) in D_2O at 20° and 0.3M NaCl.* a) *Region showing the interresidue H−C(6)/H−C(8)* (= H6/H8) (*n* + 1) *to H²−C(3′)* (= H3′2)(*n*) *cross-peaks needed for sequential assignment in the oligomer* (indicated by solid arrows on the right), *and* b) *section with intraresidue H−C(6)/H−C(8)* (= H6/H8) *to H−C(4′)* (= H4′) *NOE interactions used to link the hexitol ring proton spin system to the nucleobase at its C(2′) position* (indicated by solid arrows on the right). Extra NOE interactions, not visible in the depicted spectra but used to determine the hexitol ring conformation, are indicated by dashed arrows on the right.

and hC16) and the upfield shifted signal at 10.6 ppm to H−C(3) of hT8 and hT20. This assignment is in agreement with the strong intrastrand NOE we observed between H−C(3) of hT5 and Me of hT6 (and H−C(3) of hT17 and Me of hT18). Other imino signals were assigned by intra- and interstrand NOE cross-peaks in the Watergate NOESY spectrum schematically represented in *Fig. 5*.

All ^{31}P-NMR signals were assigned in a ^{1}H-detected ^{1}H- ^{31}P HETCOR. A full listing of all ^{1}H- and ^{31}P-resonances is given in *Table 1*.

2.4. *Conformation of the Hexitol Rings.* The hexitol ring can adopt a conformation with either an axially (chair) or an equatorially (inverse chair) oriented base moiety.

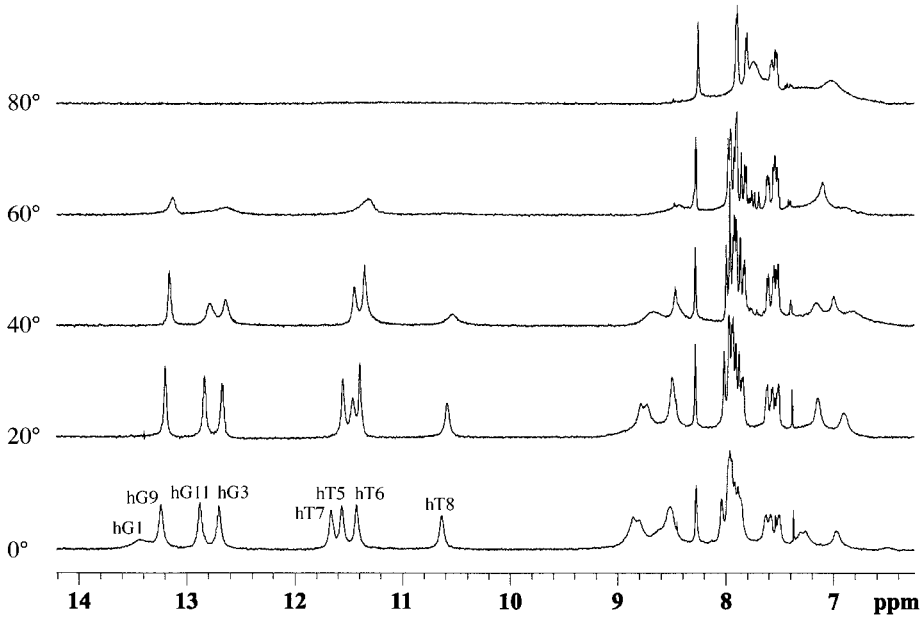

Fig. 4. *Imino- and aromatic-proton region of 'jump-return' ^{1}H-NMR spectra of 2 mM h(GCGCTTTTGCGC) in H_2O/D_2O 9:1 with 0.3M NaCl at different temperatures* (0, 20, 40, 60, and 80°)

Table 1. *Chemical Shifts* [ppm] of ^{1}*H*- and ^{31}*P-Resonances at 20°*. The $\delta(^1H)$ and $\delta(^{31}P)$ are referenced to acetate (1.92 ppm) and TMP, resp. (n.a. = not applicable).

	H–C(8)/ H–C(6)	H–C(2)/ H–C(5)	H–C(1)/ H–C(3)	H1– C(1′)	H2– C(1′)	H– C(2′)	H1– C(3′)	H2– C(3′)	H– C(4′)	H– C(5′)	H1–C(6′)/ H2–C(6′)	P
hG1/hG13	8.27	–	13.41	4.11	4.36	4.68	2.18	2.82	4.20	3.64	3.99/3.83	–
hC2/hC14	7.85	5.28	–	4.11	4.54	4.73	2.02	2.86	4.46	3.61	4.18/4.01	– 3.43
hG3/hG15	7.94	–	12.67	4.03	4.39	4.63	2.05	2.59	4.19	3.62	n.a	– 3.31
hC4/hC16	7.58	5.24	–	4.00	4.28	4.65	1.92	2.74	4.17	3.52	n.a.	– 3.61
hT5/hT17	7.88	1.69	11.46	3.92	4.43	4.52	2.00	2.70	4.35	3.55	4.18/4.02	– 3.48
hT6/hT18	7.91	1.64	11.40	3.86	4.17	4.43	1.98	2.67	4.16	3.53	n.a.	– 3.29
hT7/hT19	7.98	1.63	11.55	3.93	4.33	4.60	2.02	2.77	4.33	3.57	4.16/4.07	– 3.53
hT8/hT20	8.02	1.76	10.58	3.94	4.33	4.52	2.09	2.63	4.42	3.60	4.10/4.04	– 3.56
hG9/hG21	7.96	–	13.20	4.04	4.23	4.76	2.03	2.85	4.37	3.66	n.a./4.13	– 3.51
hC10/hC22	7.62	5.37	–	4.00	4.39	4.72	1.93	2.85	4.29	3.59	n.a.	– 3.43
hG11/hG23	7.92	–	12.67	3.97	4.51	4.57	1.99	2.61	4.05	3.61	n.a.	– 3.05
hC12/hG24	7.52	5.27	–	3.93	4.16	4.69	1.83	2.06	3.84	3.36	4.05	– 3.74

The orientation has a profound influence on duplex geometry. We have previously demonstrated that an axial orientation of the nucleobase is needed to allow HNA to hybridize strongly and selectively with RNA [17]. A HNA · RNA heteroduplex has a helical structure, very similar to the *A*-type helices of natural double-stranded nucleic acids. If the base moiety is in an equatorial position, HNA is unable to hybridize with DNA or RNA. The reason for this is the higher stabilization of the helical structure due to stacking interactions when base moieties are axially oriented, compared to the stabilization of linear structures with equatorially oriented nucleobases. However, this

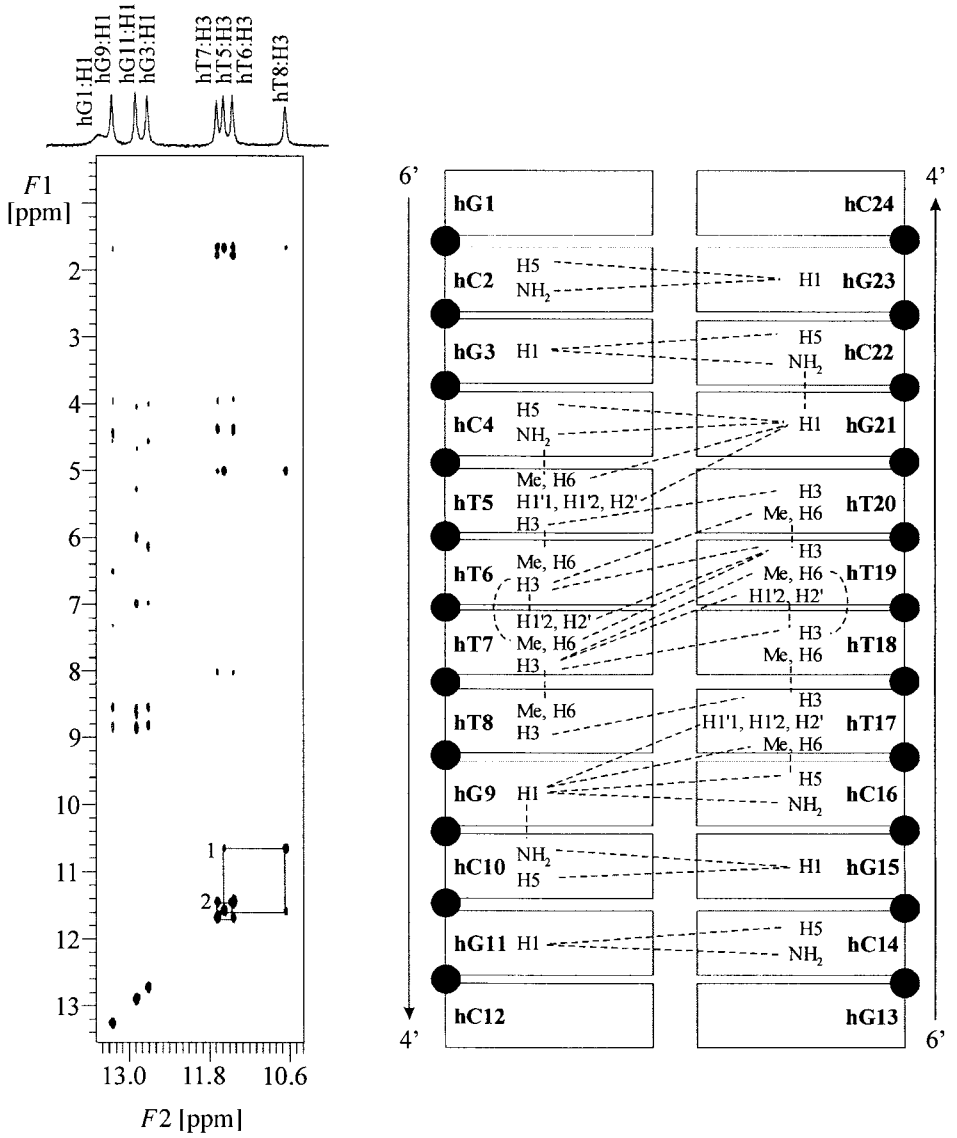

Fig. 5. *Portion of the Watergate NOESY plot measured at 0° in H_2O/D_2O 9 :1 with 0.3*M *NaCl showing the cross-peaks from the imino signals of h(GCGCTTTTGCGC)*. Boxes 1 and 2 indicate the NOE interactions of hT5 to hT20 (hT20 to hT5) and hT6 to hT19 (hT18 to hT7), respectively. Imino signals were assigned by intra- and interstrand NOE cross-peaks in the Watergate NOESY spectrum as represented schematically on the right.

does not mean that dsHNA may not adopt structures other than the typical *A*-type helix.

Before studying the overall structure, the conformation of the hexitol rings has to be verified. The strong H−C(4′)/H^1−C(3′) and H−C(4′)/H−C(5′) cross-peaks in the DQF-COSY, indicative of large active J(4′,3′1) and J(4′,5′) coupling constants,

correspond to axial positions for the three involved protons in the anhydrohexitol ring. Furthermore, very weak or non-observable cross-peaks from H–C(2′) to the axially positioned H^1–C(3′), correspond to an equatorial position for the H–C(2′) protons in the HNA strand. In the NOESY plot, there are strong intraresidue cross-peaks from the base protons H–C(8)/H–C(6) to H–C(4′) and close contacts between H^1–C(1′), H^1–C(3′), and H–C(5′). All these data correspond to anhydrohexitol rings in chair conformations with axially positioned bases (*Fig. 1, d*). This is in agreement with the previously determined conformation of monomeric [21] and dimeric [16] HNA.

2.5. *Base-Pairing in T·T Mismatches.* The observed imino signals between 10 and 12 ppm are characteristic of T·T base pairing where both H–N(3) imino protons are involved in H-bonding and in slow exchange with the surrounding H_2O. However, two different arrangements are possible for T·T wobble pairs (*Fig. 6*). In one pairing mode, the O(4) of the thymine in strand 1 extends into the major groove, and the O(4) of the thymine in strand 2 is involved in base pairing (*Fig. 6, a*), while the other pairing mode is just the opposite. Both pairing modes are present in the h(GCGCTTTTGCGC) structure (*Fig. 7*). When the O(4) of thymine is extended into the major groove, the λ angle formed by N(1) and C(2′) of this residue and C(2′) of the residue in the other strand is decreased, while λ is increased if O(4) is H-bonded (*Fig. 6* and *Table 2*). Since both pairing modes are possible, we did not include any H-bonding restraints for the four central T·T base pairs in the duplex during the structure determination. The first calculation stage of torsion-angle molecular dynamics started from two extended strands and yielded 42 accepted structures out of 100 calculated. The 25 lowest-energy structures were subjected to further refinement. Twelve refined structures showed nice base stacking for the four central wobble pairs in the duplex, despite the absence of H-bonding restraints in this part of the molecule. The mismatch pairs in the structure closest to the average of the twelve final structures are depicted in *Fig. 7, b*. Average H-bonding distances in the two outer mismatches (hT5·hT20 and hT8·hT17) are larger than those in the two central T·T wobble pairs. These increased distances correspond to the increased line broadening at 20° for the imino protons in the two outer mismatches

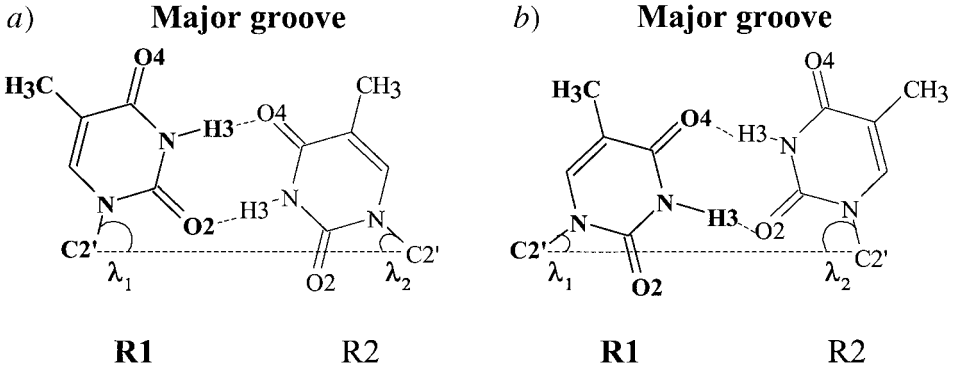

Fig. 6. *The two possible T·T wobble pairs:* a) *with H-bonds between HN(3) and O(2) of the thymine in strand 1* (R1) *and O(4) and HN(3) of the nucleobase in strand 2* (R2), *respectively, or* b) *with H-bonds between HN(3) and O(4) of the thymine in strand 1* (R1) *and O(2) and HN(3) of the nucleobase in strand 2* (R2), *respectively*

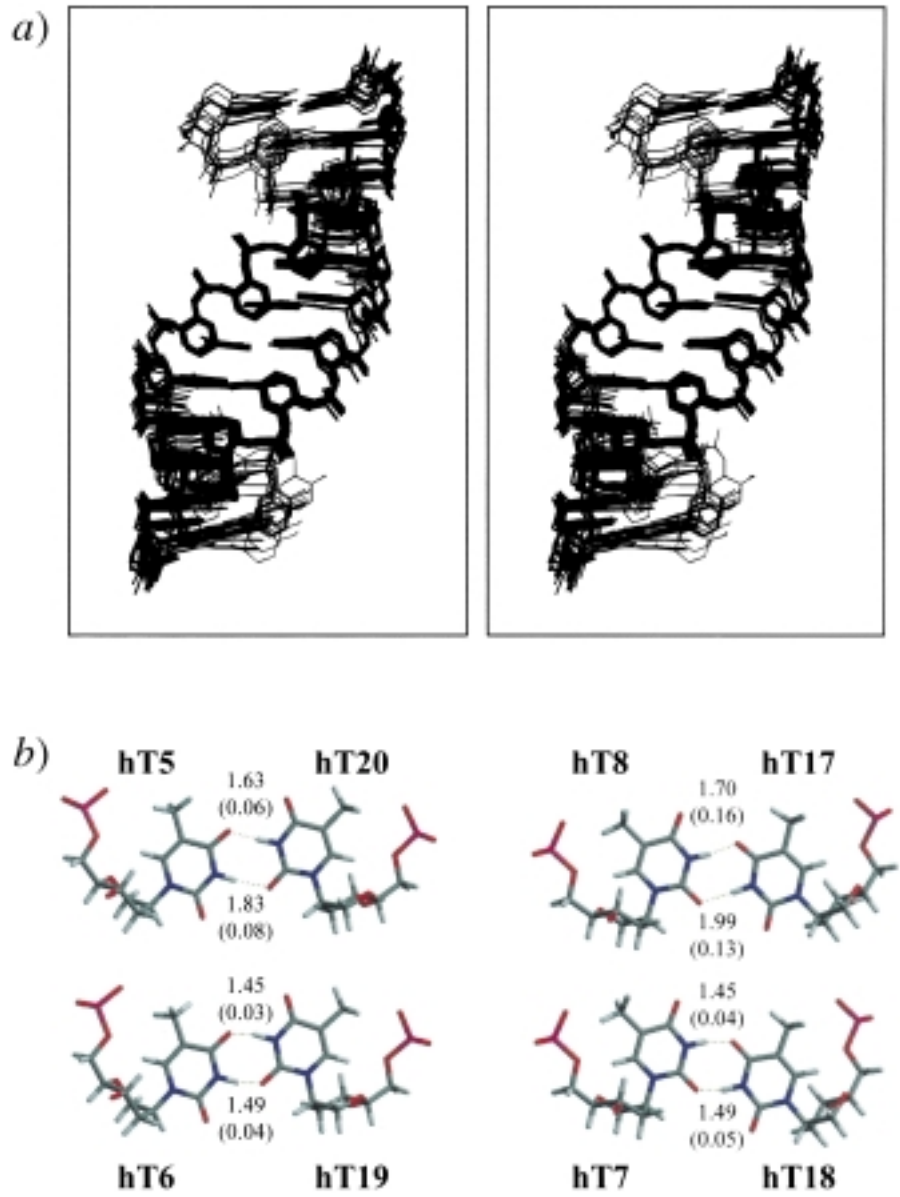

Fig. 7. a) *Overlay of the twelve accepted structures obtained from two extended strands by applying torsion-angle molecular dynamics followed by conjugate-gradient minimization without H-bonding restraints in the internal loop region* (stereo view). b) *Mismatch T·T wobble pairs in the central part of the duplex, closest to the average of the twelve refined structures that were accepted.* Average H-bonding distances are given with their standard deviations.

Table 2. *Average Values and Standard Deviations for Base-Pair Parameters in the Twelve Final Structures.* The angles λ_1 and λ_2 are defined as depicted in *Fig. 6*.

Base pair	X-displacement [Å]	C(2′) to C(2′) [Å]	λ_1 [°]	λ_2 [°]
hG1 · hC24	– 4.5 (0.3)	10.33 (0.04)	53.2 (0.3)	56.5 (1.0)
hC2 · hG23	– 4.6 (0.3)	10.34 (0.02)	55.3 (0.8)	53.3 (0.6)
hG3 · hC22	– 4.7 (0.2)	10.32 (0.02)	53.2 (0.7)	55.1 (1.1)
hC4 · hG21	– 4.6 (0.2)	10.20 (0.03)	58.3 (1.0)	53.3 (0.4)
hT5 · hT20	– 4.2 (0.3)	8.77 (0.09)	72.4 (1.1)	45.2 (1.0)
hT6 · hT19	– 4.3 (0.4)	8.20 (0.07)	80.6 (0.9)	43.3 (0.6)
hT7 · hT18	– 4.3 (0.4)	8.22 (0.08)	43.2 (0.7)	80.4 (1.2)
hT8 · hT17	– 4.3 (0.3)	8.81 (0.14)	45.6 (2.2)	72.1 (1.9)
hG9 · hC16	– 4.6 (0.2)	10.22 (0.04)	53.2 (0.3)	57.8 (0.8)
hC10 · hG15	– 4.7 (0.2)	10.32 (0.02)	55.5 (0.8)	53.4 (0.6)
hG11 · hC14	– 4.6 (0.2)	10.36 (0.02)	53.0 (0.5)	55.2 (0.5)
hC12 · hG13	– 4.6 (0.2)	10.35 (0.05)	56.5 (0.9)	53.2 (0.4)

Table 3. *Structure Statistics for the Final Set of Twelve Structures after Refinement with All Restraints*

NOE Violations (> 0.5 Å)	0
Dihedral violations (> 5°)	1 ± 1
R.m.s.d. from distance restraints [Å]	0.025 ± 0.001
R.m.s.d. from dihedral restraints [°]	0.571 ± 0.110
R.m.s.d. from average structure for all heavy atoms [Å]	0.75

compared to line-widths for other imino signals (*Fig. 4*). This line broadening is an indication of weaker H-bonding, allowing more possibility for the exchange of imino protons with the surrounding H_2O. A summary of structure statistics for accepted structures is listed in *Table 3*.

Our data confirm that four successive pyrimidine · pyrimidine base pairs can be formed within a double-stranded structure. The stability of the double-stranded structure is due to H-bonding in the mismatch region, as well as to increased base stacking for the hT7 and hT19 bases in the central part of the molecule. Therefore, the backbone of both oligonucleotide strands should come closer in the mismatch region. Due to local helix adjustments in the internal loop region, hT7 is located above hT19. This results in an extra interstrand stacking interaction compared to the central base-pair steps in the reported structures with two central U · U tandem mismatches [9] [10] (*Fig. 8*). The stacking diagrams of the latter show more similarity to the hT5 · hT20 to hT6 · hT19 (or hT17 · hT8 to hT18: · hT7) base-pair step that is flanked by the hC4 · hG21 (or hC16 · hG9) *Watson-Crick* base pair. Stacking interactions at the base-pair steps from hC4 · hG21 to hT5 · hT20 are comparable to the corresponding rC5/rU5 · rG20 to rU6 · rU19 wobble pairs (or rC17/rU17 · rG8 to rU18 · rU7) in the reported r(GGCGCUUGCGUC) [9] and r(GGACUUUGGUCC) [10] duplex structures determined by X-ray crystallography.

2.6. *Structure of the Double Helix.* The HNA dodecamer forms a double-stranded helical structure with an internal loop of four T · T wobble pairs. The overall structure is comparable to duplexes of the *A*-type family formed by natural DNA and RNA (*Fig. 9*). Superimposition of P-atoms of the structure determined by NMR onto

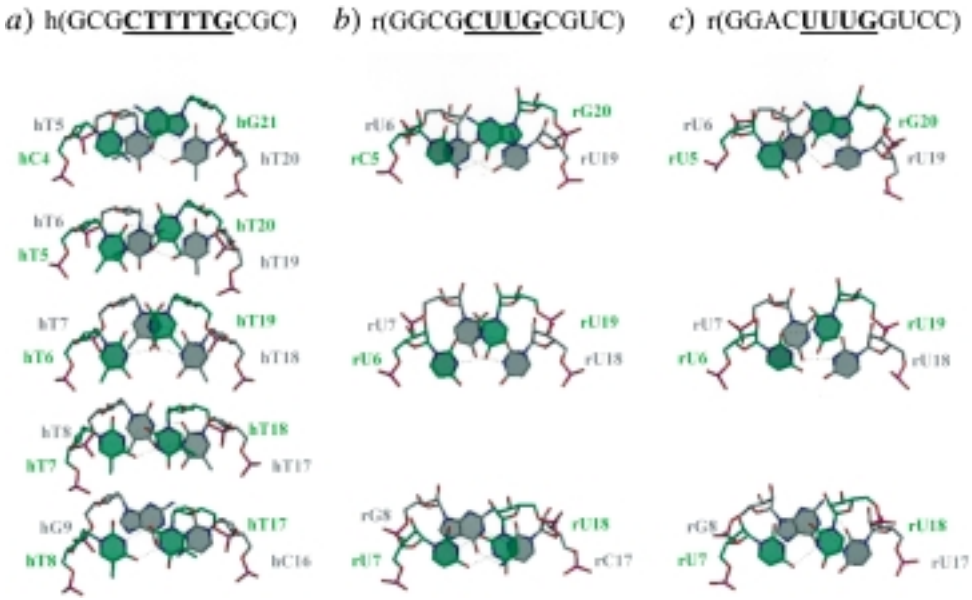

Fig. 8. *Comparison of base-stacking diagrams in the mismatch region viewed perpendicular to the mean value plane through both base pairs in each step for* a) *our HNA duplex and* b), c) *two reported RNA structures* [9] [10]. The base pairs at the top of each step have green-colored C-atoms and base planes, while these are gray-colored in the lower base pairs.

corresponding P-atoms of a canonical *A*-form RNA duplex with the same sequence (*Fig. 10*) demonstrates the influence of the central mismatches on the overall structure of h(GCGCTTTTGCGC). When all P-atoms are used in the superposition, a root mean square deviation (r.m.s.d.) of 3.6 Å is obtained. The large deviation from canonical *A*-form RNA is mainly caused by the internal loop. Superimposing the P-atoms in the G·C and T·T regions separately, yields r.m.s.d.s of 0.5 Å for regions with *Watson-Crick* pairing (green *vs.* red and blue *vs.* yellow) and 1.5 Å for the mismatch region (cyan *vs.* orange) (*Fig. 10,b* and *c*). The substitution of the five-membered ribose ring in RNA by a six-membered anhydrohexitol ring in HNA does not influence the overall *A*-type geometry of the helix in the G·C parts of the duplex. In both regions, the phosphate atoms of HNA (green and blue) and RNA (red and yellow) superimpose well, *Watson-Crick* base pairing occurs, and base stacking interactions are very similar. However, the structure of the central internal loop region of HNA (cyan) deviates substantially from that of canonical *A*-type RNA (orange). In the mismatch region, the ribbons through P-atoms in both structures deviate substantially, and compared to canonical *A*-type RNA, the T·T bases from opposite HNA strands come closer to each other, and the axial rise is increased with RNA.

The helix adjustments in the internal loop cause bending of the local helix axis in the central part of the HNA duplex, while in G·C regions, the local helix axes are rather straight and parallel to each other (*Fig. 9*). The helical axis calculated for the internal loop (base pairs hT5·hT20 to hT8·hT17) makes an angle of 25° (θ_1) with the axes calculated for each of the G·C regions. The 'swinging motion' of the helix axis in

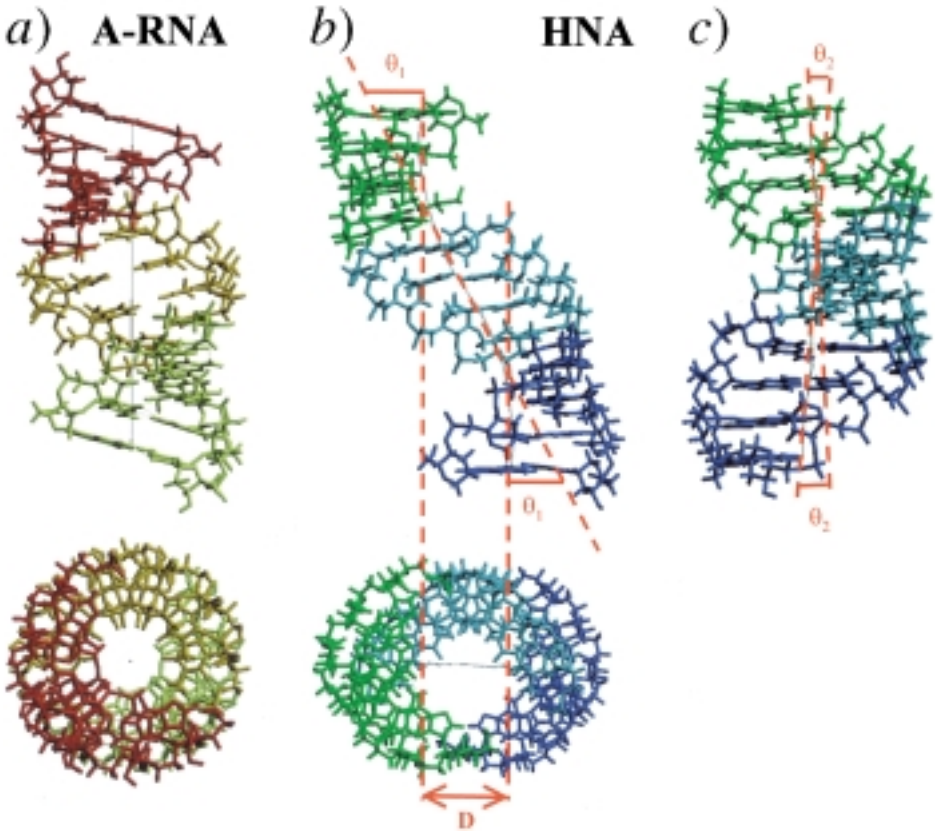

Fig. 9. *Comparison of the HNA duplex structure to a canonical dsRNA structure with the same nucleoside sequence.* a), b) *Top view and side view into the major groove for each duplex* (the helical axis calculated for the internal loop in HNA (cyan) makes an angle of 25° (θ_1) with the axis calculated for in both G · C regions (green and blue); the 'swinging motion' of the helix axis in the mismatch region causes an 8.9-Å dislocation (D) of the axis for both stems of the duplex. c) *The 10° (θ_2) twist of both stem axes relative to each other is visible in 90° rotated view of the dsHNA helix shown in* b.

the mismatch region introduces a 8.9 Å dislocation (D) between the axes for each stem of the duplex and a twist of 10° (θ_2) for the stem axes relative to each other (*Fig. 9*).

2.7. *Geometric Features of the Duplex.* 2.7.1. *Backbone Torsion Angles.* Since HNA was designed as a conformationally restricted mimic of RNA in its *A*-type conformation, it is obviously necessary to compare the structure of the HNA duplex to that of the dsRNA *A*-helical form. Deviation from the regular structure in the mismatch region is shown by comparing the present structure to that of a previously determined HNA · RNA hybrid containing only canonical base pairs and to that of the G · C base pairing regions of the dsHNA structure.

Average values for the χ, α, β, γ, δ, ε, and ζ torsion angles (*Fig. 1, b*) are listed in *Table 4*. The χ torsion angles are slightly increased compared to the average value in *A*-helical structures. The δ torsion angles in the six-membered hexitol rings center

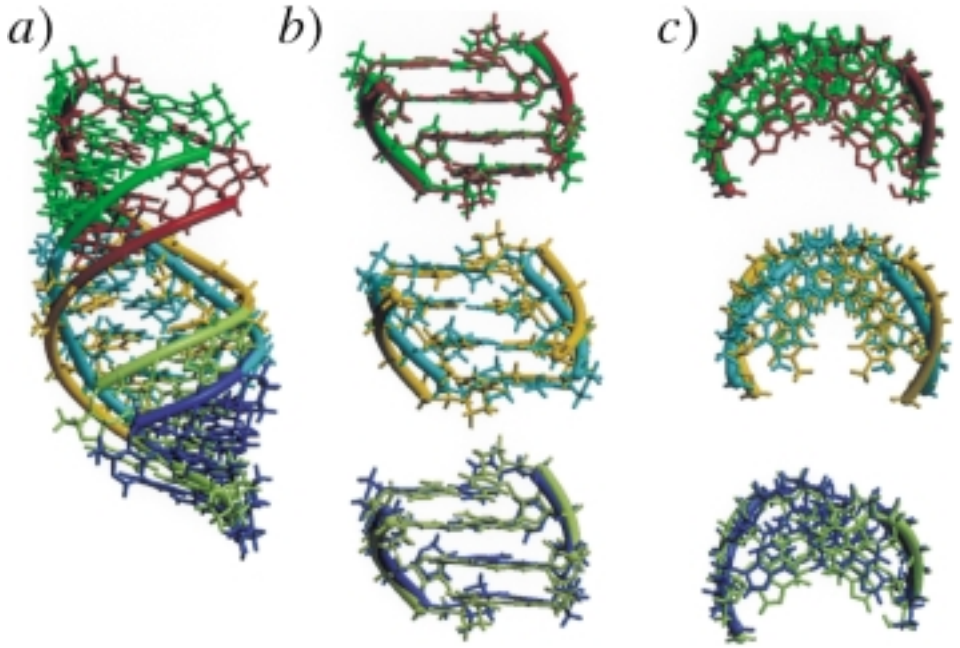

Fig. 10. *Overlay of the P-atoms of the HNA duplex to those of a canonical dsRNA structure with the same nucleoside sequence* (see *Fig. 9* for coloring scheme): a) *overlay of all P-atoms,* b) *view into the major groove, and* c) *top view when P-atoms in the top stem* (green *vs.* red), *the internal loop* (cyan *vs.* orange), *and the bottom stem* (blue *vs.* yellow) *are overlaid*

around the value of 62° compared to 82° in a five-membered C(2′)-*endo* ribose ring in *A*-type RNA. In the regions where G·C base pairing occurs, the backbone angle β deviates significantly ($>10°$, except for hG3 and hG15) from the average *A*-type dsRNA value, but remains close to the value measured in the HNA strand of the HNA·RNA heteroduplex (HNA*). In the mismatch region, several dihedral angles are altered to allow for local helix adjustments. The largest variations occur in the ε and ζ dihedral angles. There is a significant decrease in both torsion angles for hT6 (hT18) compared to the corresponding angles in the GCGC part of the duplex and HNA*. In the same base pair step (hT6·hT19 to hT7·hT18), the γ torsion angle in hT7 (hT19) is slightly increased relative to the γ torsion angles in the rest of the duplex. There is also a slight increase of the ε and ζ dihedral angles for the hC4 (hC16) residue. For the same hC4·hG21 to hT5·hT20 (hC16·hG9 to hT17·hT8) base-pair step but in the opposite strand, these angles are slightly decreased for the hT8 (hT20) residue. The γ torsion angle in hG9 (hG21) is smaller compared to the average values in HNA* and the measured values in the stem parts of the presented duplex. An enlarged ε dihedral angle occurs for hT7 (hT19), while ζ for this residue is decreased. In the same phosphodiester bridge, linking hT7 to hT8 (hT19 to hT20), the α torsion angle is significantly increased, while β is decreased relative to other torsion angles in the duplex.

It can be concluded that local geometry adjustment in the mismatch region is due to the cooperative effect of all backbone torsion angles. The smallest variation is found for

Table 4. *Average Backbone Torsion Angles* [°] *for Both Strands in the Twelve Final Structures Refined with All Experimental Restraints.* Standard deviations from average values are indicated in parentheses.

	χ	α	β	γ	δ	ε	ζ
hG1	220.0 (1.8)	–	–	–	60.9 (1.3)	213.4 (5.0)	289.7 (4.2)
hG13	219.3 (1.4)	–	–	–	60.9 (0.9)	213.9 (2.9)	288.9 (2.8)
hC2	222.5 (1.2)	299.6 (6.8)	163.6 (6.6)	64.3 (2.0)	64.9 (1.3)	215.1 (3.9)	289.1 (2.1)
hC14	222.6 (1.1)	301.7 (3.3)	162.3 (3.4)	64.7 (0.9)	65.3 (1.1)	215.6 (2.6)	290.0 (1.5)
hG3	224.5 (1.3)	289.7 (8.5)	174.8 (12.0)	62.0 (0.7)	64.0 (3.6)	217.6 (1.3)	289.5 (4.5)
hG15	224.6 (2.0)	291.7 (3.8)	172.0 (6.0)	62.2 (1.4)	63.2 (2.1)	217.4 (1.7)	288.5 (2.5)
hC4	220.7 (1.0)	301.3 (6.8)	157.4 (3.6)	64.9 (1.1)	65.0 (0.6)	221.1 (1.1)	293.7 (2.3)
hC16	221.1 (1.1)	303.3 (2.6)	156.7 (2.1)	64.5 (0.9)	64.6 (0.8)	221.6 (0.9)	292.6 (1.7)
hT5	221.9 (1.5)	296.5 (4.5)	168.4 (2.8)	62.7 (1.0)	64.4 (0.3)	216.1 (1.2)	288.6 (1.8)
hT17	221.1 (1.3)	298.8 (2.3)	167.1 (2.2)	62.3 (1.1)	64.3 (0.6)	216.4 (1.1)	287.9 (1.9)
hT6	222.8 (1.6)	298.6 (2.4)	158.4 (1.8)	63.6 (0.6)	65.5 (0.4)	204.9 (1.2)	278.9 (1.1)
hT18	221.9 (1.9)	300.0 (3.1)	158.0 (2.0)	63.4 (0.8)	65.5 (0.6)	204.9 (1.5)	279.3 (1.3)
hT7	215.7 (1.1)	298.3 (1.3)	163.2 (1.1)	66.9 (0.5)	62.2 (0.7)	234.9 (0.6)	274.7 (1.7)
hT19	215.5 (1.0)	298.8 (1.4)	163.3 (1.6)	66.8 (0.7)	62.1 (0.5)	234.8 (1.1)	274.9 (1.4)
hT8	215.4 (0.9)	316.9 (2.0)	144.4 (1.3)	64.4 (0.9)	60.0 (0.8)	212.2 (4.3)	282.9 (3.0)
hT20	215.3 (0.7)	316.8 (2.3)	144.6 (1.3)	64.4 (0.7)	60.0 (1.6)	212.2 (5.8)	283.8 (4.4)
hG9	215.0 (2.5)	200.9 (4.5)	168.5 (5.0)	58.3 (0.8)	67.2 (1.3)	218.1 (1.8)	286.5 (2.6)
hG21	214.9 (1.6)	299.3 (8.1)	170.2 (10.1)	58.0 (1.6)	67.2 (1.9)	216.5 (2.7)	287.9 (3.4)
hC10	220.4 (1.2)	306.1 (3.9)	157.8 (3.0)	64.1 (1.3)	64.8 (1.2)	214.6 (2.6)	289.5 (3.3)
hC22	221.4 (1.8)	304.2 (5.2)	160.2 (5.8)	64.4 (1.0)	65.2 (0.9)	216.0 (3.3)	290.3 (2.2)
hG11	223.4 (1.8)	298.3 (4.1)	165.8 (4.2)	62.4 (1.3)	62.9 (1.6)	220.8 (3.7)	285.6 (3.1)
hG23	224.1 (2.0)	297.0 (3.0)	165.6 (2.3)	62.4 (0.9)	63.4 (2.6)	219.8 (3.3)	288.1 (4.5)
hC12	229.4 (1.6)	305.2 (3.3)	158.5 (5.5)	62.6 (0.9)	64.9 (0.7)	–	–
hc24	229.0 (1.3)	302.6 (5.1)	160.5 (5.0)	62.5 (1.0)	64.2 (0.8)	–	–
A-RNA[a])	202	292	178	54	82	207	289
B-DNA[a])	262	314	213	36	157	155	264
HNA*[b])	222.0 (2.0)	292.8 (13.5)	163.9 (6.4)	65.3 (8.8)	67.4 (1.8)	215.6 (3.6)	289.4 (3.2)

[a]) Data for *A*-RNA and *B*-DNA are taken from *Saenger* [45]. [b]) Values listed for HNA* are average torsion angles in the HNA strand of a HNA·RNA duplex determined by NMR spectroscopy [46].

dihedral angles γ and δ, while large changes are found for the β and ε torsion angles in hT8 (hT20) and hT6 (hT18), respectively.

2.7.2. *Helical Parameters and Stacking Interactions.* To enable H-bonding between two pyrimidines in opposite strands, the distance between the C(2′) atoms of the hexitol rings to which the nucleobases are attached is reduced (*Table 2*). The minor-groove width drops from 9.9 to 8.6 Å in the hT5·hT8 (hT17·hT20) wobble pair and to 7.6 Å in the two central hT6·hT7 (hT18·hT19) mismatches (*Fig. 11*). To close the gap, the C(2′) atoms in each wobble pair move towards each other and towards the helix axis causing a reduction of the X-displacement from −4.7 Å for the C·G *Watson-Crick* pairs to −4.3 Å in the central T·T wobble pairs (*Table 2*). Similar features are reported for the crystal structure of an RNA dodecamer with tandem U·U mismatches flanked by C·G base pairs [9]. The base-pair steps in the mismatch region are different from those in regular *A*-type RNA. Axial twist and the related axial rise show an obvious change in the mismatch region of the final structures (*Fig. 11,a*). Due to the large shear in T·T wobble pairs, measurement of twist is strongly influenced by the choice of base-pair reference frame [25], which can be located either at the center of a base pair (CompDNA [26], Curves [31], RNA [27]) or either based on C(6)(Y)/C(8)(R)

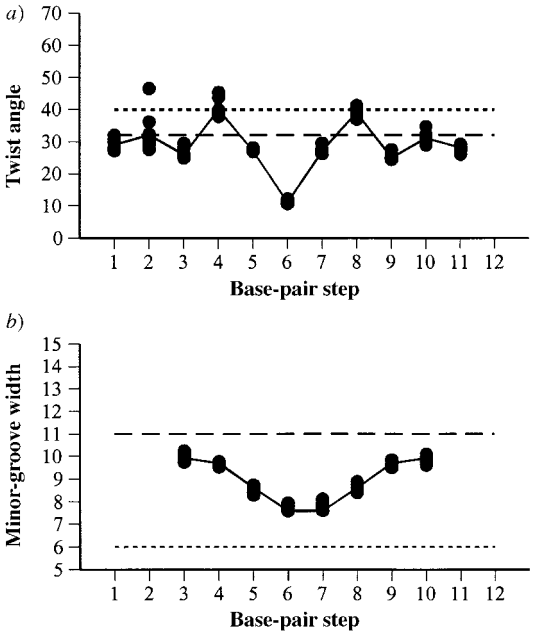

Fig. 11. *Variation of* a) *the twist angles and* b) *the minor-groove width in the twelve final structures as determined by* Curves 5.0 [31]. Average *A*- and *B*-form values are given by dashed and dotted lines, respectively. Measured averages for the twelve structures are connected by solid lines.

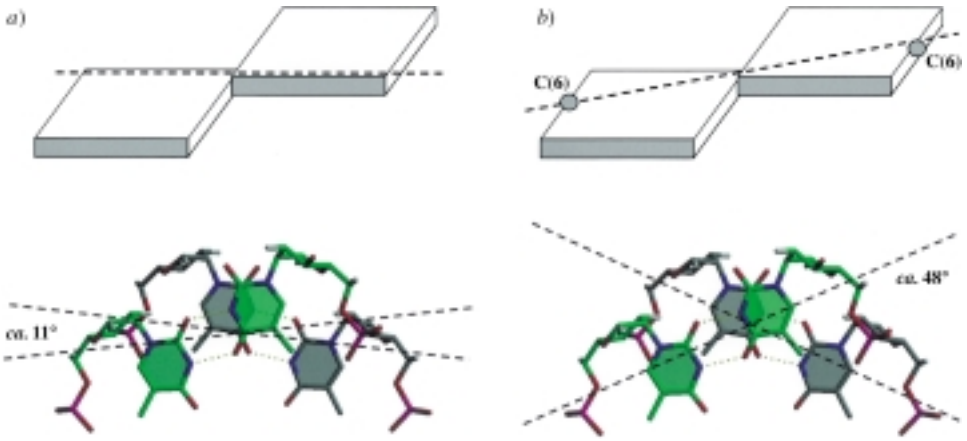

Fig. 12. *Schematic representation of the influence of a large shear on the* Y *axis in* a) *a reference frame located at the center of the base pair and* b) *a reference frame based on C(6) atoms at the outer edge of the hT·hT wobble pair.* The central hT6·hT19 to hT7·hT18 base-pair step is shown as an example of how the choice of a reference frame influences the measured twist (for coloring scheme, see *Fig. 8*).

atoms at the outer edge of a base pair (CEHS [28], FreeHelix [29], NUPARM [30]) (*Fig. 12* and *Table 5*). As with a $^{5'}_{3'}$CUUG$^{3'}_{5'}$ tandem mismatch in RNA [9], Curves5.0 [31] measures an over-winding of the helix at the $^{6'}_{4'}$CT$^{4'}_{6'}$ and $^{6'}_{4'}$TG$^{4'}_{6'}$ steps (average twist angles of

39.8 and 39.1° in HNA, 38.8 and 40.7° in RNA, PDB id 280D). This over-winding is followed by an unwinding in the next base-pair steps between two neighboring wobble pairs (average twist angles of 27.4 and 25.1° in HNA, 21.8 and 21.5° in RNA, PDB id 280D). Most striking is the increase in unwinding between the two central T·T wobble pairs in the HNA duplex (average twist angles of 9.1°).

Table 5. *Twist Angles in Each Base-Pair Step in the Structure Closest to the Average of All Accepted Structures Measured with Two Programs Using Different Reference Frames.* Values for base-pair steps in which hT·hT wobble pairs are involved are listed in italics.

	Curves 5.0	CEHS
hG1·hC24 to hC2·hG23	29.9	27.3
hC2·hG23 to hG3·hC22	32.1	32.3
hG3·hC22 to hC4·hG21	25.6	24.0
hC4·hG21 to hT5·hT20	*40.6*	*27.1*
hT5·hT20 to hT6·hT19	26.7	23.5
hT6·hT19 to hT7·hT18	*11.4*	*48.2*
hT7·hT18 to hT8·hT17	*26.8*	*22.9*
hT8·hT17 to hG9·hC16	*40.6*	*26.8*
hG9·hC16 to hC10·hG15	24.8	23.4
hC10·hG15 to hG11·hC14	30.1	30.9
hG11·hC14 to hC12·hG13	27.3	27.0

3. Conclusion. – The HNA duplex structure presented here demonstrates that an internal loop of four successive anti-parallel T·T wobble pairs can exist in an *A*-type helical structure where there is a conformationally restricted 'sugar-phosphate' backbone that favors duplex formation. The stability of the internal TTTT loop is due to the strong H-bonding and stacking interactions within the helix that remains relatively undistorted. A combination of small changes in backbone torsion angles reduces the minor-groove width, allowing T residues from opposite strands to approach each other and enabling H-bonding in T·T wobble pairs. The strongest interaction occurs in the two central T·T base pairs, as reflected in the sharp NMR signals from H-bonded imino protons in these wobble pairs and the short H-bond distances in the calculated structures. The T·T mismatches flanked by G·C *Watson-Crick* pairs have slightly longer H-bonds characterized by broader imino signals that disappear first when the temperature is increased, two spectral features that are indicative of weaker H-bonding within these wobble pairs. The central part of the h(GCGCTTTTGCGC) duplex shows striking differences in geometry. Local helix adjustments in the mismatch region give rise to a 'swinging motion' of the helix axis over the course of the HNA duplex, and an 8.9 Å displacement of the helix axes of the stems relative to each other. Conformational changes at the interface between the internal loop and both stems introduce an overall bend of 10° in the duplex.

Similar H-bonding in wobble pairs and helix adjustments have been reported for an RNA dodecamer with an internal loop of two U·U mismatches [9]. The displacement is not as pronounced since the internal loop in this structure contains only two non-standard base pairs. The strong resemblance of this RNA structure to our dsHNA structure is striking and suggests that the HNA duplex can be considered a model for

the structure of dsRNA with an internal loop of four successive U · U mismatches. The occurrence of such an RNA duplex has been described in the sequence r(GGA-CUUUUGUCC), but its structure has not been determined yet. HNA, with its conformationally rigid *N*-type building blocks, may be used as a tool to stabilize metastable RNA structures. The synthesis and study of chimeric RNA · HNA oligonucleotides may thus shed light on RNA structures of low stability and allow an analysis of the dynamics of conformational changes in RNA.

We are grateful to the K.U. Leuven for financial support (GOA 97/11). *E. Lescrinier* is a research associate of the *Fund of Scientific Research*. The authors thank Dr. *B. De Bouvere* for synthesizing the HNA monomers, Mr. *G. Schepers* for synthesizing the HNA oligonucleotide, and Dr. *A. Van Aerschot* for supervising the oligonucleotide synthesis.

Experimental Part

1. *Sample Preparation.* The HNA molecule h(GCGCTTTTGCGC) was synthesized by phosphoramidite chemistry as described previously [16].

About 5 mg of HNA dodecamer was dissolved in D_2O (0.5 ml), and the pD was adjusted to 7 by adding small amounts of 0.01N HCl in D_2O. Small amounts of NaCl were added to obtain a single structural form of the HNA molecule. After adding each aliquot of NaCl, the mixture was briefly heated to 80° and slowly cooled to r.t. to promote duplex formation. Finally, the sample was lyophilized and redissolved in D_2O (0.650 ml), yielding a soln. of 2 mM oligomer and 0.3M NaCl (pD 7). To measure imino signals, the sample was relyophilized and dissolved in H_2O/D_2O (9:1) (0.650 ml).

2. *NMR Measurements.* NMR Spectra. *Varian-500-Unity* spectrometer operating at 499.505 MHz. Quadrature detection was achieved by the *States-Haberkorn* hypercomplex mode [32]. Spectra were processed using the FELIX 97.00 software package (*Biosym Technologies*, San Diego, CA) running on a *Silicon-Graphics-Indigo2-R10000* workstation (IRIX version 6.2). The one-dimensional (1D) spectra in H_2O were recorded with a jump-return observation pulse [33]. The two-dimensional (2D) NOESY in H_2O were recorded at 0° and 20° with 50-ms mixing time using the Watergate sequence [34]. A sweep width of 11000 Hz was used in both dimensions with 64 scans, 4096 data points in t_2 and 512 FIDs in t_1. Data were apodized with a shifted sine bell square function in both dimensions and processed to a $4K \times 2K$ matrix. The 2D DQF-COSY [35], TOCSY [36], and NOESY [37] experiments (D_2O) were recorded with a sweep width of 4200 Hz in both dimensions. The residual HDO peak was suppressed by presaturation. The DQF-COSY consisted of 4096 datapoints in t_2 and 360 increments in t_1. These data were apodized with a shifted sine bell square function in both dimensions and processed to a $4K \times 1K$ matrix. Both ^{31}P-decoupled and ^{31}P-coupled spectra were recorded under the same conditions. For the TOCSY experiment, a Clean MLEV17 [38] version was used, with a low-power 90° pulse of 26.6 μs and the delay set to 69.2 μs. The total TOCSY mixing time was set to 65 ms. The spectrum was acquired with 32 scans, 2048 data points in t_2 and 512 FIDs in t_1. The data were apodized with a shifted sine bell square function in both dimensions and processed to a $4K \times 2K$ matrix. The NOESY experiments were acquired with mixing times 50, 100, 150, 200, 250, and 300 ms, 64 scans, 2048 datapoints in t_2 and 512 increments in t_1. The ^{1}H,^{31}P HETCOR [39] was recorded with 64 scans, 4096 datapoints in the proton dimension, t_2, and 400 real datapoints in the phosphorus dimension, t_1, over sweep widths of 5000 and 3000 Hz, resp. The data were apodized with a shifted sine bell square function in both dimensions and processed to a $4K \times 1K$ matrix.

3. *Structural Restraints. Distance Restraints.* The build-up curves calculated from NOESY spectra in D_2O with mixing times 50, 100, 150, and 200 ms were used to calculate 202 inter-proton distances for nonexchangeable protons. The distances H^1–C(3′)(hG1)/H^2–C(3′)(hG1) (1.75 Å), H^1–C(3′)(hG1)/H–C(5′)(hG1) and H^1–C(3′)(hC12)/H–C(5′)(hC12) (2.72 Å), H–C(5)(hC2)/H–C(6)(hC2), and H–C(5)(hC10)/H–C(6)(hC10) (2.46 Å) were used as internal references. From the Watergate NOESY spectrum at 20°, 33 NOE distance restraints involving imino protons were defined according to the same internal reference distances as mentioned above. All distance restraints were calculated with the Felix97.0 software package. Upper and lower bounds for the measured distances were set to ±20% of the calculated value. H-Bonding restraints on G · C base pairs were considered as NOE distance restraints, and no H-bonding restraints were applied in the T · T mismatch region of the molecule.

Dihedral Angle Restraints. The conformation of the anhydrohexitol rings was restrained by dihedral restraints on O′–C(1′)–C(2′)–C(3′) (60 ± 20°), C(4′)–C(2′)–C(3′)–H(3′1) (−60 ± 20°), C(2′)–C(3′)–

C(4′)–C(5′) ($60^\circ \pm 20^\circ$), C(1′)–O′–C(5′)–C(4′) ($60^\circ \pm 20^\circ$), and C(3′)–C(4′)–C(5′)–O′ ($-60^\circ \pm 20^\circ$). The backbone dihedral angle ε was restrained to $-130 \pm 40^\circ$ based on the large J(P,4′) (*ca.* 11 Hz) measured in the ^{1}H,^{31}P HETCOR spectrum. Absence of P/H^1–C(6′) and P/H^2–C(6′) crosspeaks in this spectrum, indicative for small J(P,6′1) and J(P,6′2) coupling constants, were used to restrain β to the *trans* conformation ($180 \pm 30^\circ$). The small passive couplings observed in the H^1–C(6′)/H^2–C(6′) cross-peaks in the ^{31}P-decoupled DQF-COSY were used to restrain the γ angles to $60 \pm 35^\circ$.

4. *Structure Calculation.* All structure calculations were performed with X-PLOR V3.851 [40]. The topallhdg.dna and parallhdg.dna were modified to include HNA oligonucleotides. In the topology file, the 6′-phosphorylated HNA monomers were introduced as individual residues that can be patched to each other to form an HNA oligonucleotide, comparable to the treatment of RNA and DNA in the standard X-PLOR package. Typical parameters for the hexitol ring were added to the standard parallhdg.dna parameter file.

The torsion-angle-dynamics protocol used was largely identical to that proposed for a DNA duplex [41]. A set of 100 structures was generated by torsion-angle dynamics starting from two extended strands. The torsion-angle dynamics procedure consisted of four different stages, and only in the final refinement stage, no planarity or symmetry restraints were applied. In the first stage, there was an initial search (60 ps in steps of 0.015 ps) of torsion-angle space at high temp. (2000 K) with a decreased weight on the repulsive energy term ($\omega_{vdw} = 0.1$) to facilitate rotational-barrier crossing. The coefficient for the dihedral-angle energy term ($\omega_{dihedral}$) and the NOE energy term (ω_{NOE}) were 5 and 150, resp. During the second stage (90 ps in steps of 0.015 ps), the temp. of the system was gradually reduced from 20000 to 1000 K, while ω_{vdw} was gradually increased to 1.0. The third stage was a slow cooling cartesian molecular dynamics simulation of 6 ps (with 0.003 ps timesteps). Finally, a 500-step conjugate-gradient minimization was performed with $\omega_{dihedral} = 400$ and $\omega_{NOE} = 50$.

Backbone angles and helix parameters were calculated with Curves 5.0 [31], which had been modified to handle HNA. For comparison, twist angles were recalculated with CEHS [28].

Molecule figures were generated with Bobscript2.4 [42], a modified version of Molscript1.4 [43]. *Fig. 7,b*, *8–10*, and *12* were produced with Raster3D [44].

The refined coordinates of the ten structures closest to the average are deposited in the Brookhaven Protein Data Bank (PDB ID 1EC4).

REFERENCES

[1] R. R. Gutell, 'Ribosomal RNA Structure, Evolution and Function in Protein Synthesis', CRC Press, NY, USA, 1996.
[2] R. R. Gutell, M. W. Gray, M. N. Schnare, *Nucleic Acids Res.* **1993**, *21*, 3055.
[3] R. R. Gutell, *Nucleic Acids Res.* **1994**, *22*, 3502.
[4] T. R. Cech, S. H. Damberger, R. R. Gutell, *Nat. Struct. Biol.* **1994**, *1*, 273.
[5] S. Nonin, J. L. Leroy, *J. Mol. Biol.* **1996**, *261*, 399.
[6] X. Han, J. L. Leroy, M. Gueron, *J. Mol. Biol.* **1998**, *278*, 949.
[7] J. SantaLucia, R. Kierzek, D. H. Turner, *Biochemistry* **1991**, *30*, 8242.
[8] M. Wu, J. A. McDowell, D. H. Turner, *Biochemistry* **1995**, *34*, 3204.
[9] S. E. Lietzke, C. L. Barnes, J. A. Berglund, C. E. Kundrot, *Structure* **1996**, *4*, 917.
[10] K. Baeyens, H. De Bondt, S. Holbrook, *Nature Struct. Biol.* **1995**, *2*, 56.
[11] D. R. Hare, B. Reid, *Biochemistry* **1986**, *25*, 5341.
[12] V. P. Antao, I. Tinoco Jr., *Nucl. Acids Res.* **1992**, *20,* 819.
[13] C. Richter, B. Reif, K. Wörner, S. Quant, J. P. Marino, J. Engels, C. Griesinger, H. Schwalbe, *J. Biomol. NMR* **1998,** *12*, 223.
[14] R. Micura, M. Bolli, N. Windhab, A. Eschenmoser, *Angew. Chem.* **1997**, *36*, 870.
[15] H. A. Heus, A. Pardi, *Science* **1991**, *253*, 191.
[16] H. De Winter, E. Lescrinier, A. Van Aerschot, P. Herdewijn, *J. Am. Chem. Soc.* **1998**, *120*, 5381.
[17] Y. Maurinsh, J. Schraml, H. De Winter, N. Blaton, O. Peeters, E. Lescrinier, J. Rozenski, A. Van Aerschot, E. De Clercq, R. Busson, P. Herdewijn, *J. Org. Chem*. **1997**, *62*, 2861.
[18] C. Hendrix, H. Rosemeyer, I. Verheggen, F. Seela, A. Van Aerschot, P. Herdewijn, *Chem.–Eur. J.* **1997**, *3*, 110.
[19] P. Herdewijn, H. De Winter, B. Doboszewski, I. Verheggen, K. Augustijns, C. Hendrix, T. Saison-Behmoaras, C. De Ranter, A. Van Aerschot, 'Hexopyranosyl-Like Oligonucleotides', in 'Carbohydrate Modifications in Antisense Research', Eds. Y. S. Sanghvi and P. D. Cook, American Chemical Society Symposium Series 580, Washington D.C.; 1994, p. 80.

[20] C. Hendrix, H. Rosemeyer, B. De Bouvere, A. Van Aerschot, F. Seela, P. Herdewijn, *Chem.–Eur. J.* **1997**, *3*, 1513.
[21] I. Verheggen, A. Van Aerschot, S. Toppet, R. Snoeck, G. Janssen, J. Balzarini, E. De Clercq, P. Herdewijn, *J. Med. Chem.* **1993**, *36*, 2033.
[22] I. Verheggen, A. Van Aerschot, L. Van Meervelt, J. Rozenski, L. Wiebe, R. Snoeck, G. Andrei, J. Balzarini, P. Claes, E. De Clercq, P. Herdewijn, *J. Med. Chem.* **1995**, *38*, 826.
[23] D. Gorenstein, '^{31}P-NMR, Principles and Applications', Academic Press, New York, 1984.
[24] E. P. Nikonowicz, A. Pardi, *J. Mol. Biol.* **1993**, *232*, 1141.
[25] X.-J. Lu, W. K. Olson, 'On Comparative Conformational Analysis of Nucleic Acid Structures', poster present. 11th Conversation at Albany, June 15–19, **1999** (http://rutchem.rutgers.edu/∼xiangjun).
[26] A. A. Gorin, V. B. Zhurkin, W. K. Olson, *J. Mol. Biol.* **1995**, *247*, 34.
[27] M. S. Babcock, E. P. D. Pednault, W. K. Olson, *J. Mol. Biol.* **1994**, *237*, 125.
[28] M. A. el Hassan, C. R. Calladine, *J. Mol. Biol.* **1995**, *251*, 648.
[29] R. E. Dickerson, *Nucleic Acids Res.* **1998**, *26*, 1906.
[30] M. Bansal, D. Bhattacharyya, B. Ravi, *Comput. Appl. Biosci.* **1995**, *11*, 281.
[31] R. Lavery, H. Sklenar, *J. Biomol. Struct. Dynam.* **1988**, *6,* 63.
[32] D. J. States, R. A. Haberkorn, D. J. Ruben, *J. Magn. Reson.* **1982**, *48*, 286.
[33] P. Plateau, M. Guéron, *J. Am. Chem. Soc.* **1982**, *104*, 7310.
[34] M. Piotto, V. Saudek, V. Sklenar, *J. Biomol. NMR* **1992**, *2*, 661.
[35] M. Rance, O. W. Sørensen, G. Bodenhausen, G. Wagner, R. R. Ernst, K. Wüthrich, *Biochem. Biophys. Res. Commun.* **1983**, *117*, 479.
[36] A. Bax, D. G. Davis, *J. Magn. Reson.* **1985**, *65*, 355.
[37] J. Jeener, B. H. Meier, P. Bachmann, R. R. Ernst, *J. Chem. Phys.* **1979**, *71*, 4546.
[38] C. Griesinger, G. Otting, K. Wüthrich, R. R. Ernst, *J. Am. Chem. Soc.* **1988**, *110*, 7870.
[39] V. Sklenar, H. Miyashiro, G. Zon, H. T. Miles, A. Bax, *FEBS Letters* **1986**, *208*, 94.
[40] A. T. Brünger, 'X-PLOR, in A System for X-Ray Crystallography and NMR', Yale University Press, New Haven, CT, 1992.
[41] E. G. Stein, L. M. Rice, A. T. Brünger, *J. Magn. Reson.* **1997**, *124*, 154.
[42] R. M. Esnouf, *J. Mol. Graphics* **1997**, *15*, 132.
[43] P. J. Kraulis, *J. Appl. Crystallogr.* **1991**, *24*, 946.
[44] E. A. Merritt, D. J. Bacon, *Meth. Enzymol.* **1997**, *277*, 505.
[45] W. Saenger, 'Principles of Nucleic Acid Structure', Springer-Verlag, New York, 1984.
[46] E. Lescrinier, J. Schraml, R. Busson, R. Esnouf, H. Heus, C. Hilbers, P. Herdewijn, 'Structure Determination of a HNA·RNA Hybrid by NMR Spectroscopy', in preparation.

Received February 25, 2000